CWRU-P5-00/UCSB-HEP-00-01

Exclusion Limits on the WIMP-Nucleon Cross-Section from the Cryogenic Dark Matter Search

R. Abusaidi[8], D.S. Akerib[1], P.D. Barnes, Jr.[9], D.A. Bauer[10], A. Bolozdynya[1], P.L. Brink[8], R. Bunker[10], B. Cabrera[8], D.O. Caldwell[10], J.P. Castle[8], R.M. Clarke[8], P. Colling[8], M.B. Crisler[2], A. Cummings[9], A. Da Silva[9], A.K. Davies[8], R. Dixon[2], B. Dougherty[8], D. Driscoll[1], S. Eichblatt[2], J. Emes[3], R.J. Gaitskell[9], S.R. Golwala[9,*], D. Hale[10], E.E. Haller[3], J. Hellmig[9], M.E. Huber[11], K.D. Irwin[4], J. Jochum[9], F.P. Lipschultz[7], V. Mandic[9], J.M. Martinis[4], S.W. Nam[4], H. Nelson[10], B. Neuhauser[7], M. Penn[8], T.A. Perera[1], M.C. Perillo Isaac[9], B. Pritychenko[9], R.R. Ross[3,9], T. Saab[8], B. Sadoulet[3,9], R.W. Schnee[1], D.N. Seitz[9], P. Shestople[7], T. Shutt[5], A. Smith[3], G.W. Smith[9], A.H. Sonnenschein[10], A.L. Spadafora[9], W. Stockwell[9], J.D. Taylor[3], S. White[9], S. Yellin[10], B.A. Young[6]

(CDMS Collaboration)

[1]*Department of Physics, Case Western Reserve University, Cleveland, OH 44106, USA*

[2]*Fermi National Accelerator Laboratory, Batavia, IL 60510, USA*

[3]*Lawrence Berkeley National Laboratory, Berkeley, CA 94720, USA*

[4]*National Institute of Standards and Technology, Boulder, CO 80303, USA*

[5]*Department of Physics, Princeton University, Princeton, NJ 08544, USA*

[6]*Department of Physics, Santa Clara University, Santa Clara, CA 95053, USA*

[7]*Department of Physics and Astronomy, San Francisco State University, San Francisco, CA 94132, USA*

[8]*Department of Physics, Stanford University, Stanford, CA 94305, USA*

[9]*Center for Particle Astrophysics, University of California, Berkeley, Berkeley, CA 94720, USA*

[10]*Department of Physics, University of California, Santa Barbara, Santa Barbara, CA 93106, USA*

[11]*Department of Physics, University of Colorado, Denver, CO 80217, USA*

(February 29, 2000)

Abstract

The Cryogenic Dark Matter Search (CDMS) employs Ge and Si detectors to search for WIMPs via their elastic-scattering interactions with nuclei while discriminating against interactions of background particles. CDMS data give limits on the spin-independent WIMP-nucleon elastic-scattering cross-section that exclude unexplored parameter space above 10 GeV c^{-2} WIMP mass and, at $> 84\%$ CL, the entire 3σ allowed region for the WIMP signal reported by

the DAMA experiment.

PACS numbers: 95.35.+d, 14.80.-j, 14.80.Ly

Extensive evidence indicates that a large fraction of the matter in the universe is nonluminous, nonbaryonic and "cold" – nonrelativistic at the time matter began to dominate the energy density of the universe [1–3]. Weakly Interacting Massive Particles (WIMPs) are an excellent candidate for nonbaryonic, cold dark matter [4,2]. Minimal supersymmetry provides a natural WIMP candidate in the form of the lightest superpartner, with a typical mass $M \sim 100$ GeV c^{-2} [5–8]. WIMPs are expected to have collapsed into a roughly isothermal, spherical halo within which the visible portion of our galaxy resides. WIMPs scatter off nuclei via the weak interaction, potentially allowing their direct detection [9,10]. The expected spectrum of recoil energies (energy given to the recoiling nucleus during the interaction) is exponential with a characteristic energy of a few to tens of keV [11]. The expected event rate is model-dependent but is generically 1 kg^{-1} d^{-1} or lower [10].

This Letter reports new exclusion limits on the spin-independent WIMP-nucleon elastic-scattering cross-section by the Cryogenic Dark Matter Search (CDMS). The rate of rare WIMP-nucleon interactions is constrained by extended exposure of detectors that discriminate WIMP-induced nuclear recoils from electron recoils caused by interactions of background particles [12,13].

The ionization yield Y (the ratio of ionization production to recoil energy in a semiconductor) of a particle interaction differs greatly for nuclear and electron recoils. CDMS detectors measure phonon and electron-hole pair production to determine recoil energy and ionization yield for each event. The data discussed here were obtained with two types of detectors, Berkeley Large Ionization- and Phonon-mediated (BLIP) and Z-sensitive Ionization- and Phonon-mediated (ZIP) detectors [12–17]. For both types, the drift field for the ionization measurement is supplied by radially-segmented electrodes on the faces of the disk-shaped crystals [18]. In BLIP detectors, phonon production is determined from the detector's calorimetric temperature change. In ZIP detectors, athermal phonons are collected to determine phonon production and xy-position. Detector performance is discussed in detail elsewhere [14,16,17].

Photons cause most bulk electron recoils, while low-energy electrons incident on the detector surfaces cause low-Y electron recoils in a thin surface layer ("surface events"). Neutron, photon, and electron sources are used to determine efficiencies for discrimination between nuclear recoils and bulk or surface electron recoils. Above 10 keV, CDMS detectors reject bulk electron recoils with $> 99\%$ efficiency and surface events with $> 95\%$ efficiency. CDMS detectors that sense athermal phonons provide further surface-event rejection based on the differing phonon pulse shapes of bulk and surface events [17]. This phonon-based surface-event rejection alone is $> 99.7\%$ efficient above 20 keV.

The 1-cm-thick, 7-cm-diameter detectors are stacked 3 mm apart with no intervening material. This close packing enables the annular outer ionization electrodes to shield the disk-shaped inner electrodes from low-energy electron sources on surrounding surfaces. The probability that a surface event will multiply scatter is also increased.

The low rate of WIMP interactions necessitates operation at a site with low background-particle flux. CDMS detectors are operated beneath 16 meters-water-equivalent overburden, which stops the hadronic component of cosmic-ray air showers and reduces the muonic component by a factor of 5. A custom, radiopure extension to a modified Oxford S-400 dilution refrigerator provides a low-background 20 mK volume [19].

Several layers of shielding surround the cryostat. Outermost is a $> 99.9\%$ efficient

plastic-scintillator veto to detect muons and thus allow rejection of muon-coincident particles. Inside the veto, a 15-cm-thick lead shield reduces the background photon flux by a factor of 1000. A 1-cm-thick shield made of ancient lead provides additional photon shielding inside the cryostat [20]. Samples of all construction materials were screened to ensure low radioactive contamination. The measured event rate below 100 keV due to photons is roughly 60 keV^{-1} kg^{-1} d^{-1} overall and 2 keV^{-1} kg^{-1} d^{-1} anticoincident with veto.

Neutrons with energies capable of producing keV nuclear recoils are produced by muons interacting inside and outside the veto ("internal" and "external" neutrons, respectively). The dominant, low-energy (< 50 MeV) component of these neutrons is moderated by a 25-cm thickness of polyethylene between the outer lead shield and cryostat [21]. However, high-energy external neutrons may punch through the moderator. A simulation of these neutrons assumes the production spectrum given in [22] and propagates them through the shield to the detectors. The accuracy of the simulation's propagation of neutrons is confirmed by the excellent agreement of the simulated and observed recoil-energy spectra due to veto-coincident and calibration-source neutrons. A large fraction of the external neutrons are vetoed: $\sim$40% due to neutron-scintillator interactions and an unknown fraction due to associated hadronic showers. This unknown fraction, combined with a factor of $\sim$4 uncertainty in the production rate, makes it difficult to accurately predict the absolute flux of unvetoed external neutrons. However, normalization-independent predictions of the simulation, such as relative rates of single scatters and multiple scatters, relative rates in Si and Ge detectors, and the shapes of nuclear-recoil spectra, are insensitive to reasonable changes in the neutron spectrum.

Two data sets are used in this analysis: one consisting of 33 live days taken with a 100 g Si ZIP detector between April and July, 1998, and another taken later with Ge BLIP detectors. The Si run yields a 1.6 kg d exposure after cuts. The total low-energy electron surface-event rate is 60 kg^{-1} d^{-1} between 20 and 100 keV. Four nuclear recoils are observed in the Si data set. Based on a separate electron calibration, the upper limit on the expected number of unrejected surface events is 0.26 events (90% CL). These nuclear recoils also cannot be due to WIMPs. Whether their interactions with target nuclei are dominated by spin-independent or spin-dependent couplings, WIMPs yielding the observed Si nuclear-recoil rate would cause an unacceptably high number of nuclear recoils in the Ge data set discussed below. Therefore, the Si data set, whose analysis is described elsewhere [23], measures the unvetoed neutron background.

Between November, 1998, and September, 1999, 96 live days of data were obtained using 3 of 4 165 g Ge BLIP detectors. One detector is discarded because it displays a high rate of veto-anticoincident low-energy electron surface events, 230 kg^{-1} d^{-1} as compared to 50 kg^{-1} d^{-1} for the other detectors (10 to 100 keV). This detector suffered additional processing steps that may have contaminated its surface and damaged its electrodes. Data-quality, nuclear-recoil acceptance, and veto-anticoincidence cuts reduce the exposure (mass $\times$ time) by 45%. To take advantage of close packing, analysis is restricted to events fully contained in the inner electrodes, reducing the exposure further by a factor of 2.5 to yield a final Ge exposure of 10.6 kg d [24].

Figure 1 shows a plot of ionization yield vs. recoil energy for the Ge data set. Bulk electron recoils lie at ionization yield $Y \simeq 1$. Low-energy electron events form a distinct band at $Y \sim 0.75$, leaking into the nuclear-recoil acceptance region below 10 keV.

Figure 2 displays the recoil-energy spectrum of unvetoed nuclear recoils for the Ge data set. Only single scatters (events triggering a single detector) are shown; the WIMP multiple-scatter rate is negligible. An analysis threshold of 10 keV, well above trigger thresholds, is imposed. This choice reduces the data set's sensitivity but simplifies analysis by rendering low-energy electron misidentification negligible. The nuclear-recoil efficiency is determined using calibration-source neutrons and its stability is monitored using veto-coincident neutrons. Thirteen unvetoed nuclear recoils are observed in the 10.6 kg d exposure between 10 and 100 keV; this rate is similar to that expected for the WIMP signal claimed by the DAMA experiment [25,26]. However, much evidence indicates that the CDMS nuclear recoils are caused by neutrons rather than WIMPs.

Figure 3 displays a scatter plot of ionization yields for multiple scatters. The observation of 4 Ge multiple-scatter nuclear recoils is the primary evidence for the neutron interpretation. It is highly unlikely that these events are misidentified low-energy electron events. Figures 1 and 3 demonstrate excellent separation of low-energy electron events from nuclear recoils. Analysis using events due to electrons emitted by the contaminated detector yields an upper limit of 0.05 misidentified multiple-scatter low-energy electron events (90% CL).

All other pieces of evidence are also consistent with the neutron interpretation. First, the 4 nuclear recoils observed in the Si data set cannot be interpreted as WIMPs or surface events. Second, there is reasonable agreement between predictions from the Monte Carlo simulation and the relative observed numbers of 4 Ge multiple scatters, 4 Si single scatters, and 13 Ge single scatters. Normalizing the simulation by the 17 total Ge nuclear-recoil events yields 2.7 expected Si single scatters and 1.3 expected Ge multiple scatters. Statistically, the expected neutron background should result in a less likely combination of Ge single scatters, Ge multiple scatters, and Si single scatters 23% of the time. Finally, a Kolmogorov-Smirnov test indicates that the deviation between the observed and simulated nuclear-recoil spectral shapes would be larger in 28% of experiments.

The 90% CL excluded region for the WIMP mass M and the spin-independent WIMP-nucleon elastic-scattering cross-section σ is derived using an extension of the approach of Feldman and Cousins [29]. The above arguments require accounting for the component of the observed Ge single scatters (with energies $E_{\rm i}$) that is due to the unvetoed neutron flux n. This flux is constrained by the number $N_{\rm m}$ of multiple scatters in Ge and the number $N_{\rm Si}$ of nuclear recoils in Si. To determine the 90% CL excluded region in the plane of M and σ alone, the parameter n is projected out. For a grid of physically allowed values of M, σ, and n, the expected distribution of the likelihood ratio $R = \mathcal{L}(E_i, N_{\rm m}, N_{\rm Si}|\,\sigma, M, \tilde{n})/\widehat{\mathcal{L}}$ is calculated by Monte Carlo simulation in order to determine the critical parameter R_{90} such that 90% of the simulated experiments have $R > R_{90}$. Here $\tilde{n}$ is the value of n that maximizes the likelihood $\mathcal{L}$ for the given parameters M and σ and the observations. $\widehat{\mathcal{L}}$ is the maximum of the likelihood for any physically allowed set of parameters. The WIMP-nucleon cross-section σ is converted to a WIMP-nucleus cross-section assuming A^2 scaling with target nuclear mass. This scaling is valid for models of supersymmetric WIMPs currently favored [5–8]. The 90% CL region excluded by the observed data set, with ratio $R_{\rm data}$, consists of all parameter space for which $R_{\rm data} \leq R_{90}$. Figure 4 displays the lower envelope of points excluded for all values of n. Because all the nuclear recoils may be neutron scatters, $\sigma = 0$ is not excluded.

This limit excludes new parameter space for WIMPs with $M > 10$ GeV c^{-2}, some of which is allowed by supersymmetry [7]. The data are compatible with the DAMA/NaI-0 ex-

clusion limit based on pulse-shape analysis [27]. However, these data exclude, at $> 84\%$ CL, the entire region allowed at 3σ by the DAMA/NaI-1 to 4 annual modulation signal [25]. This region, given by the $v_0 = 220$ km s^{-1} curve in Figure 4a of Ref. [25], is used because it is determined solely from the annual modulation signal. The data presented here also exclude the analogous 2σ allowed region for DAMA/NaI-1 to 2 at $> 96\%$ CL [26]. Although without theoretical support, non-A^2 scaling may allow the two results to be compatible.

We thank Paul Luke of LBNL for his advice regarding surface-event rejection. We thank the engineering and technical staffs at our respective institutions for invaluable support. This work is supported by the Center for Particle Astrophysics, an NSF Science and Technology Center operated by the University of California, Berkeley, under Cooperative Agreement No. AST-91-20005, by the National Science Foundation under Grant No. PHY-9722414, by the Department of Energy under contracts DE-AC03-76SF00098, DE-FG03-90ER40569, DE-FG03-91ER40618, and by Fermilab, operated by the Universities Research Association, Inc., under Contract No. DE-AC02-76CH03000 with the Department of Energy.

REFERENCES

* Corresponding author: golwala@cfpa.berkeley.edu

[1] V. Trimble, Annu. Rev. Astron. Astrophys. **25**, 425 (1987).
[2] P. J. E. Peebles, *Principles of Physical Cosmology* (Princeton University Press, Princeton, NJ, 1993).
[3] K. A. Olive and D. N. Schramm, Eur. J. Phys. C **3**, 119 (1998).
[4] B. W. Lee and S. W. Weinberg, Phys. Rev. Lett. **39**, 165 (1977).
[5] G. Jungman, M. Kamionkowski, and K. Griest, Phys. Rep. **267**, 195 (1996).
[6] J. Ellis, T. Falk, K. A. Olive, and M. Schmitt, Phys. Lett. B **413**, 355 (1997).
[7] J. Edsjo and P. Gondolo, Phys. Rev. D **56**, 1879 (1997).
[8] A. Bottino, F. Donato, N. Fornengo, and S. Scopel, hep-ph/0001309, submitted to Phys. Rev. D.
[9] M. W. Goodman and E. Witten, Phys. Rev. D **31**, 3059 (1985).
[10] J. R. Primack, D. Seckel, and B. Sadoulet, Annu. Rev. Nucl. Part. Sci. **38**, 751 (1988).
[11] J. D. Lewin and P. F. Smith, Astropart. Phys **6**, 87 (1996).
[12] T. Shutt *et al.*, Phys. Rev. Lett. **69**, 3531 (1992).
[13] T. Shutt *et al.*, Phys. Rev. Lett. **69**, 3425 (1992).
[14] R. Gaitskell *et al.*, in *Proceedings of the Seventh International Workshop on Low Temperature Detectors*, edited by S. Cooper (Max Planck Institute of Physics, Munich, 1997).
[15] K. D. Irwin *et al.*, Rev. Sci. Instr. **66**, 5322 (1995).
[16] R. M. Clarke *et al.*, in *Proceedings of the Second International Workshop on the Identification of Dark Matter*, edited by N. J. C. Spooner and V. Kudryavtsev (World Scientific, Singapore, 1999).
[17] R. M. Clarke *et al.*, preprint SU/BC99-170.
[18] T. Shutt *et al.*, to appear in Nucl. Instrum. Meth. **A**, (2000).
[19] J. D. Taylor *et al.*, Adv. Cryo. Eng. **41**, 1971 (1996).
[20] A. Da Silva *et al.*, Nucl. Instrum. Meth. **A 364**, 578 (1995).
[21] A. Da Silva *et al.*, Nucl. Instrum. Meth. **A 354**, 553 (1995).
[22] F. F. Khalchukov, A. S. Mal'gin, V. G. Ryassny, and O. G. Ryazhskaya, Nuovo Cimento **6C**, 320 (1983).
[23] R. Abusaidi *et al.*, in preparation.
[24] R. Abusaidi *et al.*, in preparation.
[25] R. Bernabei *et al.*, preprint ROM2F/2000/01 and INFN/AE-00/01.
[26] R. Bernabei *et al.*, Phys. Lett. B **450**, 448 (1999).
[27] R. Bernabei *et al.*, Phys. Lett. B **389**, 757 (1996).
[28] L. Baudis *et al.*, Phys. Rev. D **59**, 022001 (1999).
[29] G. J. Feldman and R. D. Cousins, Phys. Rev. D **57**, 3873 (1998).

FIGURES

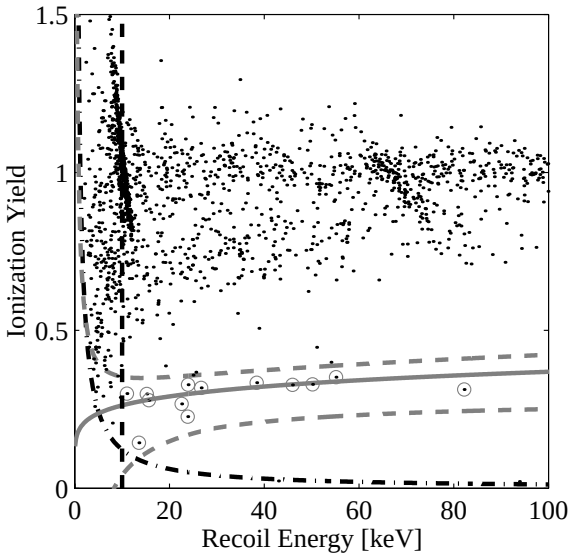

FIG. 1. Ionization yield (Y) vs. recoil energy for veto-anticoincident single scatters contained in the inner electrodes of the 3 uncontaminated Ge detectors. Solid curve: expected position of nuclear recoils. Dashed curves: nominal 90% nuclear-recoil acceptance region. Dashed line: 10 keV analysis threshold. Dashed-dotted curve: threshold for separation of ionization signal from amplifier noise. Circled points: nuclear recoils. The presence of 3 events just above the acceptance region is compatible with 90% acceptance.

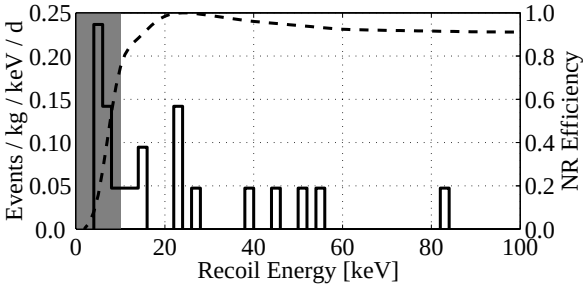

FIG. 2. Solid: histogram of nuclear recoils observed in the inner electrodes of the 3 uncontaminated Ge detectors (left-hand scale). Shaded: 10 keV analysis threshold. Dashed: peak-normalized nuclear-recoil efficiency (right-hand scale).

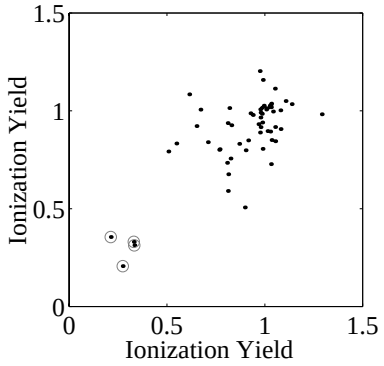

FIG. 3. Scatter plot of ionization yields for multiple scatters in the 3 uncontaminated Ge detectors with at least 1 inner-electrode scatter and both scatters between 10 and 100 keV. Circled events are tagged as nuclear recoils in both detectors. Bulk recoils and surface events lie at $Y \simeq 1$ and $Y \sim 0.75$, respectively.

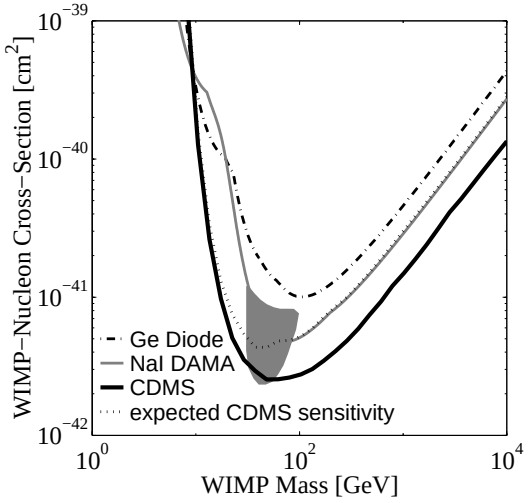

FIG. 4. Spin-independent σ vs. M. The regions above the curves are excluded at 90% CL. Solid dark curve: limit from this analysis. Dotted curve: CDMS expected sensitivity (median simulated limit) given the observed neutron background. Because the number of multiple scatters observed is larger than expected, the limit from this analysis is lower than the median simulated limit. Solid light curve: DAMA limit using pulse-shape analysis [27]. Shaded region: DAMA 3σ allowed region as described in text [25]. Dashed-dotted curve: Ge diode limit, dominated by [28]. All curves are normalized following [11], using the Helm spin-independent form-factor, A^2 scaling, WIMP characteristic velocity $v_0 = 220$ km s^{-1}, mean Earth velocity $v_E = 232$ km s^{-1}, and $\rho = 0.3$ GeV c^{-2} cm^{-3}.